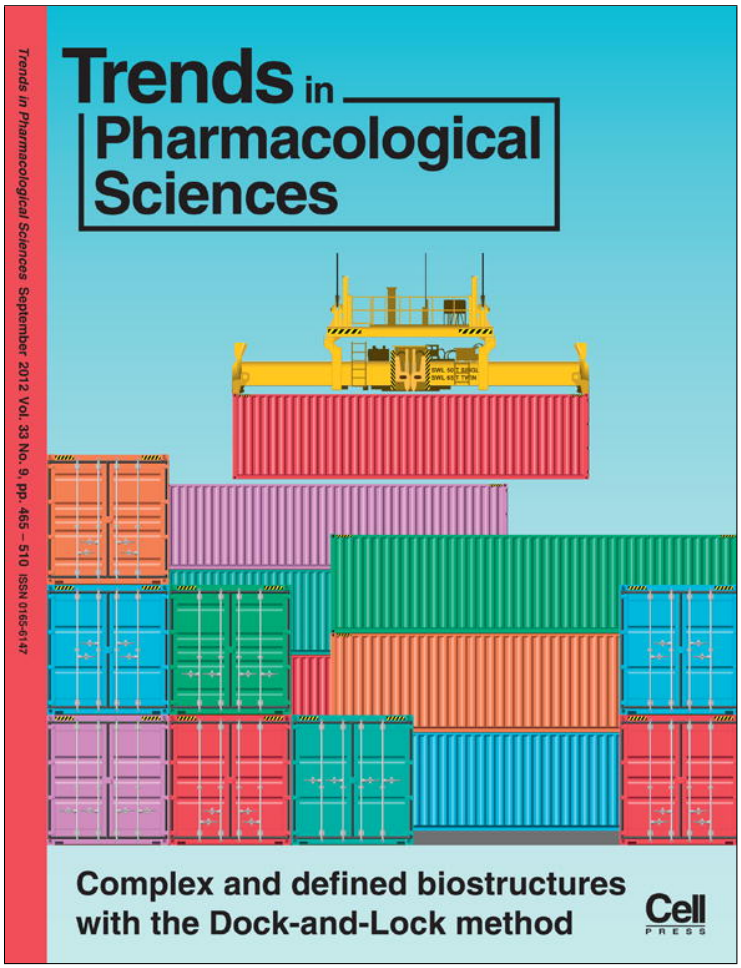

Review

Size matters in activation/inhibition of ligand-gated ion channels

Juan Du, Hao Dong and Huan-Xiang Zhou

Department of Physics and Institute of Molecular Biophysics, Florida State University, Tallahassee, FL 32306, USA

Cys loop, glutamate, and P2X receptors are ligand-gated ion channels (LGICs) with 5, 4, and 3 protomers, respectively. There is now growing atomic level understanding of their gating mechanisms. Although each family is unique in the architecture of the ligand-binding pocket, the pathway for motions to propagate from ligand-binding domain to transmembrane domain, and the gating motions of the transmembrane domain, there are common features among the LGICs, which are the focus of the present review. In particular, agonists and competitive antagonists apparently induce opposite motions of the binding pocket. A simple way to control the motional direction is ligand size. Agonists, usually small, induce closure of the binding pocket, leading to opening of the channel pore, whereas antagonists, usually large, induce opening of the binding pocket, thereby stabilizing the closed pore. A cross-family comparison of the gating mechanisms of the LGICs, focusing in particular on the role played by ligand size, provides new insight on channel activation/inhibition and design of pharmacological compounds.

Common threads of LGICs

As with change in transmembrane voltage, ligand binding is a common stimulus for ion channels. The term LGICs often specifically refers to three families of ionotropic receptors: Cys loop receptors [in particular, nicotinic acetylcholine receptors (nAChRs)], ionotropic glutamate receptors (iGluRs), and P2X receptors (P2XRs). The functional units of these receptors are all oligomers comprising identical or homologous protomers, but the numbers of protomers differ (Figure 1) [1–3]. Cys loop receptors, iGluRs, and P2XRs have 5, 4, and 3 protomers, respectively. In each family, the minimum construct for channel function consists of an extracellular domain (to be referred to as the ligand-binding domain, or LBD) that harbors the ligand-binding sites, and a transmembrane domain (TMD) that contains the pore for ion permeation, with additional domains that play other functional roles such as regulation of channel activity and trafficking. The ligand-binding sites are located in the interprotomer interfaces for Cys loop receptors and P2XRs, but in the cleft between two lobes of each LBD protomer for iGluRs (Figure 1). With a significant amount of structural and mechanistic knowledge accumulated for each family of LGICs, it now seems appropriate to look for common lessons.

A common set of questions that define the gating mechanisms of all the LGICs is: What rearrangement of the binding sites does ligand binding induce? How are the motions of the LBD propagated to the TMD? And what are the motions of the pore-lining helices that are responsible for pore opening/closing? Given their distinct molecular architectures, the three families of LGICs are expected to have different solutions to these questions. However, as suggested recently [4], the different LGICs could have some common elements in their gating mechanisms. The gating mechanisms provide the basis for understanding ligand actions and designing pharmacological compounds. This review focuses on ligand size as a common factor in affecting ligand actions on the three families of LGICs.

Significant advance in the understanding of the gating mechanisms of Cys loop receptors and iGluRs was made by comparing the structures of the LBDs bound with various agonists and antagonists. For Cys loop receptors, this was made possible by the fact that the LBD is homologous to a water-soluble, homopentameric acetylcholine-binding protein (AChBP) [5]. For iGluRs, this was made possible by constructs in which the TMD is removed, and the open

Glossary

Mutant cycle analysis: a way to obtain information on the contribution of the interaction between two neighboring residues to channel gating, by studying the effects of mutating these residues. The perturbations of the two single mutations and the double mutation on the free energy difference between open and closed states of the channel (from measuring single channel dwell times) are obtained. A significant deviation of the effect of the double mutation from the sum of the effects of the two single mutations indicates the importance of the interaction between the two residues in channel gating.

Normal mode analysis: a modeling approach to obtain functionally important conformational changes of a protein. The motions of the protein are modeled as harmonic. By solving an eigenvalue problem, harmonic modes are obtained. Typically, some of the low frequency modes, which involve collective motions of a large fraction of the atoms, are assumed to be associated with biological function.

Rate equilibrium free energy relation: a way to assess whether the environment of a residue in the transition state for channel opening is more similar to that in the closed state or that in the open state. Mutations on the residue are made and their effects on the activation energy for channel opening and on the free energy difference between open and closed states are obtained. The former are then expressed as a fraction of the latter. A fraction close to 0 indicates that the environment of the residue in the transition state is similar to that in the closed state; a fraction close to 1 indicates that the environment of the residue in the transition state is similar to that in the open state.

Substituted cysteine accessibility method: a given residue in a channel protein is mutated into cysteine and a cysteine modifying agent is then applied in the absence and presence of an agonist. The change in modification rates is interpreted as indicating whether the residue becomes more or less accessible upon channel activation.

Targeted molecular dynamics simulation: a part of a protein is forced to move in a given direction, and the goal is to see how the rest of the protein responds in the simulation. In particular, a part of the ligand-binding domain may be moved to mimic the motion induced by an agonist, and the response of the transmembrane domain may suggest a gating mechanism.

Corresponding author: Zhou, H-X. (hzhou4@fsu.edu).

 0165-6147/$ – see front matter http://dx.doi.org/10.1016/j.tips.2012.06.005 Trends in Pharmacological Sciences, September 2012, Vol. 33, No. 9

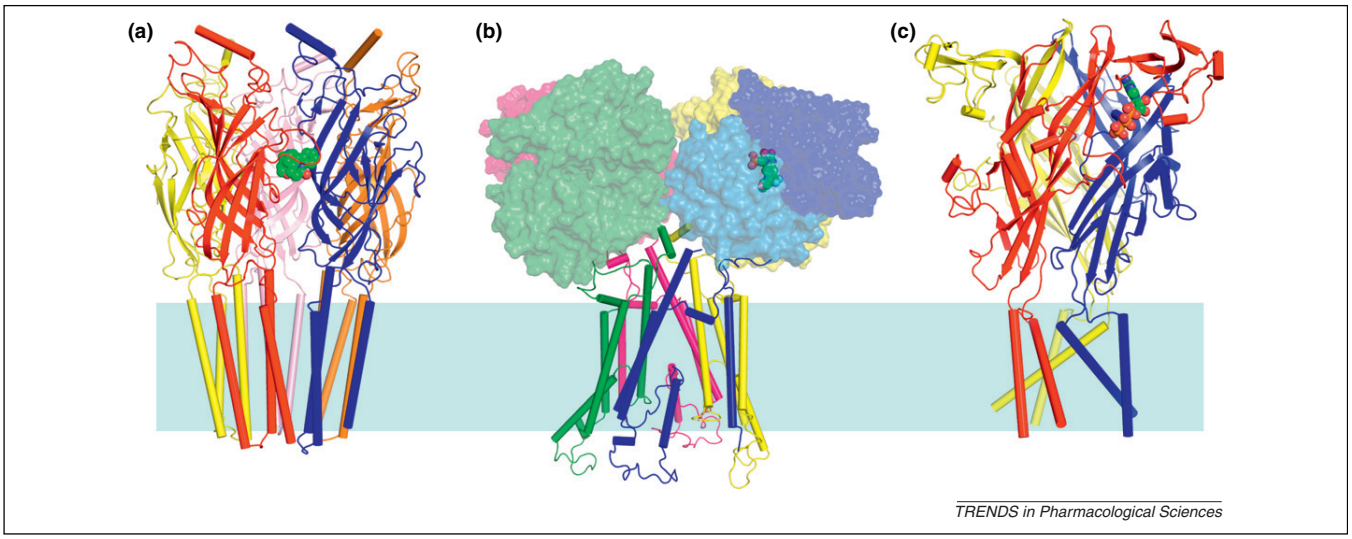

Figure 1. Structures of three families of ligand-gated ion channels. The protomers in each receptor are shown in different colors; ligands are shown as spheres. **(a)** Torpedo acetylcholine receptor in the apo form [Protein Data Bank (PDB) entry 2BG9] [1]. The M3–M4 linker and M4 are not shown. Strychnine, an antagonist, is built into the binding site by superimposing against PDB entry 2XYS [9]. **(b)** GluR2 α-amino-3-hydroxyl-5-methyl-4-isoxazole propionic acid (AMPA) receptor bound with antagonist ZK 200775 (PDB entry 3KG2) [2]. In chain A (front right), the two lobes of the ligand-binding domain are shown as dark (D1) and light (D2) blue surfaces. Chain B (front left) is in green. **(c)** Zebra fish P2X4 receptor in the apo form (PDB entry 3H9V) [3]. ATP in the 'distal' orientation, which was suggested to stabilize the closed state by molecular dynamics simulations [4], is built into the putative binding site.

ends are then connected by a short peptide linker [6,7]. By comparing the iGluR LBD structures bound with agonists, partial agonists, and competitive antagonists, Armstrong and Gouaux [7] observed that agonists induce significant cleft closure, partial agonists do so to a lesser extent, and antagonists keep the LBD in the open cleft conformation. Hansen *et al*. [8] similarly observed that the AChBP C loop closes down on a nAChR agonist but opens up when an antagonist is bound. This observation was confirmed recently by a comparison of AChBP structures bound with various agonists and antagonists [9].

In developing a model for nAChR activation and inhibition, it was further observed that small ligands can fit better into a closed-down binding pocket, whereas larger ligands can fit better into an opened-up binding pocket, leading to the conclusion that agonists tend to be small and antagonists tend to be large [10]. As shown below, a systematic analysis of the available AChBP and iGluR LBD structures generally supports this conclusion. Although no antagonist-bound structure is yet available for any P2XR, structural models obtained from molecular dynamics simulations [4] suggest that the same conclusion may extend to P2XRs as well. It seems that ligand size is a key determinant in the activation/inhibition of all the three families of LGICs. Agonists, usually small, induce closure of the binding pocket, leading to opening of the channel pore, whereas competitive antagonists, usually large, induce opening of the binding pocket, thereby stabilizing the closed channel pore. This review pays only passing attention to inverse agonists, which close spontaneously open channels, and allosteric modulators, which bind the receptors at sites distinct from the agonist-binding sites.

Cys loop receptors

In addition to nAChRs, the Cys loop family also includes 5-hydroxytryptamine (5-HT), γ-aminobutyric acid, and glycine receptors, and glutamate-gated chloride channels (GluCl); the first two are cation-selective, whereas the last three are anion-selective. In the LBD, each protomer comprises two β-sheets (Box 1). The C loop, connecting β9 and β10 in the outer sheet, moves a considerable distance to accommodate the bound ligand (Figure 2a). At the apex of the C loop is a pair of adjacent Cys residues (at positions 189 and 190 in the homomeric neuronal α7 nAChR) that form a disulfide bond. Among 31 AChBP structures in the Protein Data Bank (PDB), the distances between the first C loop Cys residues of two neighboring protomers ($d_{Cys-Cys}$) span a wide range, from 35.5 to 48.4 Å (Table 1). A shorter interprotomer $d_{Cys-Cys}$ signifies closing down of the C loop, whereas a longer $d_{Cys-Cys}$ signifies opening up of the C loop. Confirming previous observations [8,9], histograms in $d_{Cys-Cys}$ (Figure 2b) show that agonist-bound structures tend to have the C loop closed down, antagonist-bound structures tend to have the C loop opened up, and partial agonist-bound structures have intermediate opening of the C loop.

The information in Table 1 also provides support to the notion that small ligands fit better into a closed-down binding pocket, whereas larger ligands fit better into an opened-up binding pocket [10]. Among 27 structures bound with nonpeptide ligands, there is a moderate correlation (R^2 = 0.48) between $d_{Cys-Cys}$ and ligand molecular weight (Figure 2c). The peptide ligands have much higher molecular weights (although in each case much of the molecular weight may be positioned outside the ligand-binding pocket) and correspond to larger $d_{Cys-Cys}$ values, further buttressing the trend.

The outliers in the correlation plot of Figure 2c are interesting. In PDB 2XNV, the ligand is 2-[2-(4-phenylpiperidin-1-yl)ethyl]-1H-indole (compound 6 from an *in silico* screening) (Figure 2d), an α7 nAChR antagonist [11]. The bound ligand adopts a wedge-shaped conformation, with the indole and phenyl rings forming the two adjoining faces. The indole ring is stacked against the C loop of

the protomer on the 'principal' side, whereas the phenyl ring is stacked against strand β2 (in particular residue Y53, corresponding to α7 W54) of the protomer on the 'complementary' side. [On the principal side, ligands are commonly found to contact several aromatic residues, including Y92, W148, Y187, and Y194, as well as C190 (α7 numbering) at the apex of the C loop (Box 1).] The wedge shape, with the tips of the two apposing rings ~7 Å apart, allows the ligand to expend a minimal number of atoms to achieve a significant opening of the C loop. The ligand in PDB 2XNT, (2s)-2-[(4-chlorobenzyl)oxy]-2-phenylethanamine, behaves in much the same way. Again, a wedge-shaped ligand is positioned as if to pry open the interprotomer interface.

By contrast, the situation is very different in the structure of AChBP bound with lobeline (PDB 2BYS) [8], an agonist (Figure 2e). The bound lobeline adopts an extended conformation, with the two terminal phenyl rings maximally separated from each other. The slender ligand is positioned nearly vertically, with the midsection surrounded by the C loop on the principal side and by β2 Y53 on the complementary side. The two terminal phenyl rings form additional interactions: one positioned at the top interacting with the complementary side and the other positioned at the bottom interacting with the principal side. Lobeline thus distributes its atoms away from the C loop, explaining why a relatively high molecular weight ligand can still reside entirely in a binding pocket with a

Box 1. Sequences and functionally important motifs in three families of LGICs

The sequence alignment of several AChBPs and the LBDs of several Cys loop receptors is as follows:

```
                    α1                  β1                  β2
Ac AChBP     6 RLKSDLFN--RSPMYPGPTKDDPLTVTLGFTLQDIVKVDSSTNEVDLVYYEQQRWKLNSLMWD-PNEYGNI
Bt AChBP     4 WTLLNQITG--ESDVIPLSNNTPLNVSLNFKLMNIVEADTEKDQVEVVLWTQASWKVPYYSSLLSS--SSL
Ls AChBP     4 ADILYNIRQTSRPDVIPTQRDRPVAVSVSLKFINILEVNEITNEVDVVFWQQTTWSDRTLAWN-SS--HSP
α7 nAChR     5 KLYKELVKNYNPLERPVANDSQPLTVYFSLSLLQIMDVDEKNQVLTTNIWLQMSWTDHYLQWN-VSEYPGV
nAChR α      6 RLVANLLENYNKVIRPVEHHTHFVDITVGLQLIQLINVDEVNQIVETNVRLRQQWIDVRLRWN-PADYGGI
5-HT3A      40 RLSDHLLANYKKGVRPVRDWRKPTTVSIDVIMYAILNVDEKNQVLTTYIWYRQYWTDEFLQWT-PEDFDNV
                β3          β4          β5    β5'    β6    β6'   Cys loop    β7
Ac AChBP    74 TDFRTSAADIWTPDITAYSSTRPV-QVLSPQIAVVTHDGSVMFIPAQRLSFMCDPTGVDS-EEGVTCAVKF
Bt AChBP    71 DQVSLPVSKMWTPDLSFYNAIAAP-ELLSADRVVVSKDGSVIYVPSQRVRFTCDLINVDT-EPGATCRIKV
Ls AChBP    72 DQVSVPISSLWVPDLAAYNAISKP-EVLTPQLARVVSDGEVLYMPSIRQRFSCDVSGVDT-ESGATCRIKI
α7 nAChR    75 KTVRFPDGQIWKPDILLYNSADERFDATFHTNVLVNSSGHCQYLPPGIFKSSCYIDVRWFPFDVQHCKLKF
nAChR α     76 KKIRLPSDDVWLPDLVLYNNADGDFAIVHMTKLLLDYTGKIMWTPPAIFKSYCEIIVTHFPFDQQNCTMKL
5-HT3A     110 TKLSIPTDSIWVPDILINEFVDVG-KSPNIPYVYVHHRGEVQNYKPLQLVTACSLDIYNFPFDVQNCSLTF
                β8                        β9          C loop      β10
Ac AChBP   143 GSWVYSGFEIDLK----TD-TDQVDLSSYYA-SSKYEILSATQTRQVQHYSCCPE-PYIDVNLVVKFRE
Bt AChBP   140 GSWTHDNKQFALI----TGEEGVVNIAEYFD-SPKFDLLSATQSLNRKKYSCCEN-MYDDIEITFAFRK
Ls AChBP   141 GSWTHHSREISVD----PT-TENSDDSEYFSQYSRFEILDVTQKKNSVTYSCCPE-AYEDVEVSLNFRK
α7 nAChR   146 GSWSYGGWSLDLQ-------MQEADISGYIP-NGEWDLVGIPGKRSERFYECCKE-PYPDVTFTVTMRR
nAChR α    147 GIWTYDGTKVSIS----PE-SDRPDLSTFME-SGEWVMKDYRGWKHWVYYTCCPDTPYLDITYHFIMQR
5-HT3A     180 TSWLHTIQDINITLWRSPE-EVRSDKSIFIN-QGEWELLEVFPQFKEFS-IDISN-SYAEMKFYVIIRR
```

The LBD has 10 β-strands per protomer. β1, β2, β3, β5, and β6 form the inner sheet, with the remaining four strands (β4, β7, β9, and β10) forming the outer sheet. The loop connecting β9 and β10 is commonly referred to as C loop; the loop connecting β6 and β7 has a conserved pair of disulfide-bonded Cys residues (orange letters), and is referred to as the Cys loop, which is the namesake for the protein family. Ligands are commonly found to contact C190 (orange letter; α7 numbering) at the apex of the C loop and several aromatic residues, including Y92, W148, Y187, and Y194 on the principal side and W54 on the complementary side (green letters; α7 numbering).

The TMD of a Cys loop receptor has four α-helices per protomer; M2 lines the pore. The β1–β2 loop, Cys loop, and M2–M3 linker are positioned at the LBD–TMD interface [1,16–18], and are involved in propagating motions from the LBD to the TMD (Box 2).

The sequence and domain separation of the GluR2 AMPA receptor are shown below:

```
393 (D1)
KTVVVTTILESPYVMMKKNHEMLEGNERYEGYCVDLAAEIAKHCGFKYKLTIVGDGKYGARDADTKIWNGM
                                  495 (D2)                    522 (M1)
VGELVYGKADIAIAPLTITLVREEVIDFSKPFMSLGISIMIKKPQKSKPGVFSFLDPLAYEIWMCIVFAYI
                                568 (M2)                    595 (M3)
GVSVVLFLVSRFSPYEWHTEEFEDGRETQSSESTNEFGIFNSLWFSLGAFMQQGCDISPRSLSGRIVGGVW
                617   621     625       632 (D2)
WFFTLIIISSYTANLAAFLTVERMVSPIESAEDLSKQTEIAYGTLDSGSTKEFFRRSKIAVFDKMWTYMRS
                                                            732 (D1)
AEPSVFVRTTAEGVARVRKSKGKYAYLLESTMNEYIEQRKPCDTMKVGGNLDSKGYGIATPKGSSLGTPVN
          757 (D2)                          789 (M4)
LAVLKLSEQGLLDKLKNKWWYDKGECGAKDSGSKEKTSALSLSNVAGVFYILVGGLGLAMLVALIEFCYK
```

The LBD consists of two lobes, D1 and D2, as indicated by dark and light blue letters in the sequence. In the resting state structure [2] (Figure 1b), the pore-lining M3 helices are longer by four residues in the 'proximal' (chains A and C) protomers than in the 'distal' (chains B and D) protomers. The C-terminal portion of the M3 helix contains the conserved SYTANLAAF motif and the channel gate.

Box 1 (*Conitued*).

The sequence alignment of zP2X4R with rat P2X1 to P2X3 receptors is given below:

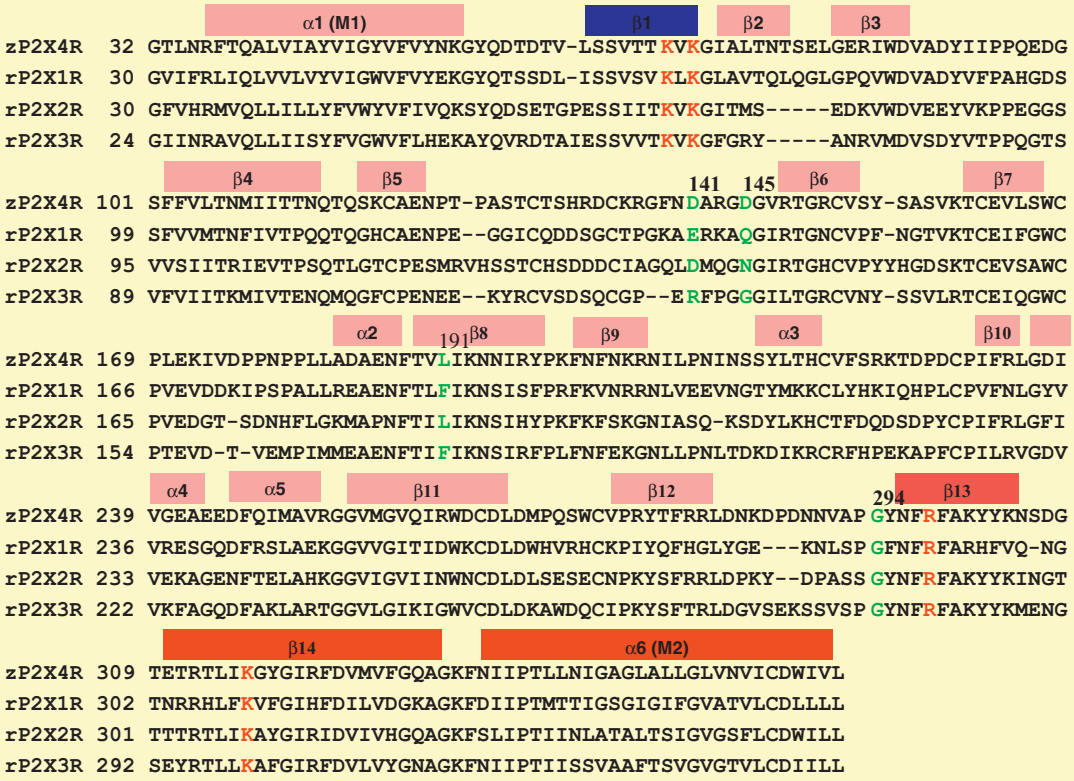

Four conserved charge residues (red letters) putatively interact with the triphosphate group of bound ATP. Several other positions implicated in ligand interactions are highlighted in green. The M2 helix lines the channel pore.

closed C loop. Clearly, ligand size alone has its limitation in predicting ligand action. Reinforcing this point, a ligand can change from a partial agonist for one receptor subtype to a full or 'super' agonist for another receptor subtype [12], or even from a competitive antagonist for the wild type channel to an agonist for a mutant channel [13]. In addition, some competitive antagonists can also act, perhaps with the same mechanism of action, as inverse agonists for constitutively active mutant channels [14].

Although the most noticeable conformational change induced by agonists and antagonists is the movement of the C loop, in some agonist-bound structures, the rest of the LBD also seems to undergo conformational change (Figure 2a). In particular, the outer β-sheet appears to undergo a clockwise rotation (top view) around an axis that divides the two β-sheets. Based, in part, on a comparison between the 4-Å electron microscopy structure of the heteromeric muscle nAChR in the apo form and the structure of carbamylcholine-bound AChBP (PDB 1UV6; [15]), Unwin [1] proposed that the clockwise rotation is involved in channel activation. Recently, the structures of two bacterial homologs, ELIC and GLIC, of Cys loop receptors were determined [16–18]. Putatively ELIC is in the closed state and GLIC is in the open state. Because ELIC and GLIC have low sequence identity (~20%), there is no unique way to align their structures, and different alignments have led to varying speculations on the motions of the extracellular domain that may trigger channel opening [17–20]. In particular, Zimmermann and Dutzler [19] suggested that a counterclockwise rotation, opposite to what was proposed by Unwin [1], of the extracellular domain leads to channel opening. Computational studies have also produced an assortment of models for LBD motions [10,20–26].

The structures of ELIC and GLIC do unequivocally show that the external end of the pore-lining M2 helix undergoes an outward tilt to open the pore [17,18]. That an M2 tilt constitutes the gating motion is supported by functional studies [27,28] and by a recent structure of a GluCl channel in the putative open state [29]. So for Cys loop receptors, there is now broad consensus that agonist-induced channel activation begins with the closing down of the C loop and ends with the outward tilt of the M2 helix. However, what additional motions are involved in between and how the motions are propagated remain unsettled [30,31] (Box 2).

Glutamate receptors

iGluRs are divided into three main subtypes: α-amino-3-hydroxyl-5-methyl-4-isoxazole propionic acid (AMPA), *N*-methyl-D-aspartate (NMDA), and kainate receptors. In 2009, the structure of a nearly full-length AMPA receptor (GluR2 homomeric) in the antagonist-bound form was determined [2]. This structure reveals that the LBD is a dimer of dimers, with limited contact between the dimers,

whereas the TMD has 4-fold symmetry, with helix M3 lining the pore (Figure 1b). All other iGluR structures in the PDB are for the isolated LBD (in dimeric form), with the most entries for the GluR2 AMPA receptor. In each protomer, the LBD consists of two lobes, referred to as D1 and D2, that form a clamshell structure (Figure 3a). Depending on the ligand bound at the interlobe cleft, the opening of the clamshell, as measured by the distance ($d_{K410–K695}$) between residue K410 near the tip of D1 and residue K695 near the tip of D2 (GluR2 numbering; Box 1), varies widely, from 24.7 to 31.0 Å (Table 1). As observed by Armstrong and Gouaux [7], agonists close the clamshell to a greater extent than partial agonists, whereas antagonists keep the clamshell open (Figure 3a,b).

Here again ligand size appears to be a determinant for the extent of the binding pocket opening. There is reasonable correlation ($R^2 = 0.58$) between $d_{K410–K695}$ and ligand molecular weight (Figure 3c). The trends shown by the histograms of Figure 3b and the correlation plot of Figure 3c for the GluR2 AMPA receptor are also seen for kainate receptors (there are too few NMDA receptor LBD structures in the PDB for statistical analysis). For both nAChRs and iGluRs, it takes ~70 Da of ligand molecular weight to increase the binding pocket opening by 1 Å.

Based on a comparison of the GluR2 LBD dimer structures bound with either an agonist (AMPA) or an antagonist (DNQX), Sun *et al.* [32] speculated that agonist-induced closure of the clamshell moves the tip of the D2 lobe away from the central axis, and this opens the channel pore. The structure of the nearly full-length GluR2 AMPA receptor in the resting state [2] showed that the outward movement of the D2 tip would drag the M3–D2 linker, which in turn pulls the M3 helix outward. Moreover, at the level of the M3–D2 linkers, the diagonal pair of protomers (chains B and D) distal to the central axis moves much more than the proximal pair (chains A and C), and hence contributes more to channel activation. Atomistic details of how agonist binding induces channel opening are revealed by targeted molecular dynamics simulations (see Glossary) [33]. The resulting activation model explains many observations in functional studies, in particular the correlation between the extent of ligand-induced LBD closure and the degree of channel activation [7,34] (Box 2).

LGICs become desensitized in the sustained presence of an agonist. For iGluRs, significant structural information is available for the desensitized state (this is in contrast to the lack of such information for Cys loop receptors). Desensitization involves the disruption of the D1–D1 dimeric interface [35–37]. A model for the LBD dimer in the desensitized state was created by introducing a disulfide bond in the D2–D2 dimeric interface (which leads to separation of the D1–D1 dimeric interface) [36]. Targeted molecular dynamics simulations showed that the separation of the D1–D1 dimeric interface pushes the D2–M3 linkers inward,

Table 1. Ligands bound to two types of ligand-binding domains

Ligand	Molecular weight	PDB	Ligand type	Distance (Å)	Refs
AChBPs[a]					
Acetylcholine	146.2	2XZ5	Agonist	36.4	[80]
Carbamylcholine	147.2	1UV6	Agonist	37.6	[15]
Anabaseine	160.2	2WNL	Agonist	36.7[b]	[81]
Nicotine	162.2	1UW6	Agonist	36.5	[15]
Epibatidine	208.7	2BYQ	Agonist	35.9	[8]
CAPS	221.3	2BJ0	Buffer	35.5	[82]
Designed compound 1	231.3	2Y54	Agonist	39.1	[58]
HEPES	238.3	1I9B	Buffer	37.8	[5]
Clothianidin	249.7	2ZJV	Agonist	37.2	[83]
Thiacloprid	252.7	3C84	Agonist	37.6	[84]
Imidacloprid	255.7	3C79	Agonist	38.1	[84]
Compound 18 (*in silico* screening)	261.8	2XNT	Antagonist	44.5	[11]
Tropisetron	284.4	2WNC	Partial agonist	38.7	[81]
4-OH-DMXBA	294.4	2WN9	Partial agonist	42.0	[81]
Compound 6 (*in silico* screening)	304.4	2XNV	Antagonist	45.0	[11]
DMXBA	308.4	2WNJ	Partial agonist	38.0	[81]
Strychnine	334.4	2XYS	Antagonist	40.7	[9]
Designed compound 4	335.4	2Y57	Agonist	38.1	[58]
Lobeline	337.5	2BYS	Agonist	36.3	[8]
In silico compound 31	348.5	2W8F	Antagonist	43.3	[57]
Designed compound 3	351.4	2Y56	Agonist	39.9	[58]
Designed compound 6	366.5	2Y58	Agonist	38.2	[58]
In silico compound 35	410.6	2W8G	Antagonist	44.9	[57]
Gymnodimine A	509.7	2X00	Antagonist	41.7	[85]
d-Tubocurarine	610.7	2XYT	Antagonist	43.0	[9]
Methyllycaconitine	682.8	3SIO	Antagonist	44.8	[86]
13-Desmethyl spirolide C	694.0	2WZY	Antagonist	45.0	[85]
α-Conotoxin IMI	12 resi	2BYP	Antagonist	48.4	[8]
α-Conotoxin PnIA(A10L D14K)	16 resi	2BR8	Antagonist	48.3	[87]
α-Cobratoxin	71 resi	1YI5	Antagonist	44.6	[88]
		3SQ9	apo	41.9	[89]

Table 1 (*Continued*)

Ligand	Molecular weight	PDB	Ligand type	Distance (Å)	Refs
GluR2 LBD[c]					
Glutamate	147.1	2GFE	Agonist	25.6	[90]
(S)-Des-Me-AMPA	172.1	1MQD	Agonist	24.9	[91]
(R)-5-HPCA	184.2	3PD9	Agonist	25.7	[92]
(S)-7-HPCA	184.2	3PD8	Agonist	25.3	[92]
AMPA	186.2	1P1Q	Agonist	26.0	[93]
Quisqualate	189.1	1MM7	Agonist	25.6	[94]
(R)-TDPA	189.2	3BFU	Agonist	24.8	[95]
(S)-TDPA	189.2	3BFT	Agonist	25.4	[95]
Willardiine	199.2	1MQJ	Partial agonist	25.7	[34]
Kainate	213.2	1GR2	Partial agonist	26.5	[6]
ACPA	214.2	1M5E	Agonist	26.1	[96]
Fluoro-willardiine	217.2	1MQI	Partial agonist	25.8	[34]
(S)-ATPA	227.2	1NNP	Agonist	26.5	[97]
Chloro-willardiine	233.6	3RTF	Partial agonist	26.3	[98]
(S)-4-AHCP	238.2	1WVJ	Agonist	26.2	[99]
(S)-CPW399	239.2	1SYH	Agonist	25.5	[100]
Nitro-willardiine	244.2	3RTW	Partial agonist	26.2	[98]
(S)-Thio-ATPA	244.3	2AIX	Agonist	26.4	[101]
DNQX	250.1	1LB9	Antagonist	28.0	[32]
Br-HIBO	251.0	1M5C	Agonist	24.7	[96]
2-Me-Tet-AMPA	254.2	1M5B	Agonist	25.9	[96]
Bromo-willardiine	278.1	1MY3	Partial agonist	26.2	[102]
(S)-ATPO	322.3	1N0T	Antagonist	28.1	[103]
Iodo-willardiine	325.1	1MQG	Partial agonist	26.1	[34]
2-Bn-Tet-AMPA	330.3	2P2A	Agonist	27.0	[104]
Compound 28	366.3	3R7X	Antagonist	31.0	[105]
ZK 200775	409.3	3KG2	Antagonist	30.1	[2]
(S)-NS1209	518.6	2CMO	Antagonist	28.6	[106]

[a]The protein in 3SQ9 is a chimera of *Lymnaea stagnalis* AChBP and the LBD of α7 nAChR; the protein in 3SIO is a chimera of *Aplysia californica* AChBP and the LBD of α7 nAChR. The proteins in the remaining entries are AChBPs from *Lymnaea stagnalis*, *Aplysia californica*, or *Bulinus truncatus*. Seven other PDB entries containing AChBPs were not used for a variety of reasons [noncompetitive interactions (2PGZ and 2PH9); C loop disorder (2Y7Y) or asymmetry (2BYN, 2XZ6, 3GUA, and 3T4 M)]. Distance listed in column 5 is $d_{Cys-Cys}$, calculated as the average over the pentamer. Nine other PDB entries were discarded because they contained ligands identical to those listed above; the retained entries have representative $d_{Cys-Cys}$ values.

[b]Only two of the five ligand-binding sites in 2WNL are bound with the cyclic form of anabaseine, which acts as a nAChR agonist. The interprotomer Cys–Cys distance was calculated after replicating one of the two protomers, whose C loops are in contact with a cyclic ligand, to the positions of the other three protomers.

[c]Distance listed in column 5 is $d_{K410-K695}$, calculated on the first chain (typically chain A) of a dimer. In total, 35 other PDB entries were discarded because they contained ligands identical to those listed above; the retained entries have representative $d_{K410-K695}$ values.

thus largely reversing the motions seen during channel activation and leading to the closing of the pore [33].

P2X receptors

In mammals there are seven subtypes of P2XRs, denoted as P2X1 to P2X7 receptors. From a structural point of view, P2XRs have been the least well characterized among the three families of LGICs, but the recent determination of the zebrafish P2X4 receptor (zP2X4R) in the apo form [3] (Figure 1c) is changing the situation [38,39]. Previous mutational studies [40–45] identified four conserved charged residues, K70, K72, R298, and K316 (zP2X4R number; Box 1), as part of the ATP-binding site. These four residues are clustered at the interprotomer interface, with K70 and K72 on strand β1 of one protomer, and R298 on strand β13 and K316 on strand β14 of another (Figure 4); β1 and β14 are connected to TMD helices M1 and M2, respectively, the latter lining the pore (Figure 1c). Recent functional studies have illuminated the gating mechanism of P2XRs. The channel gate is located at the external portion of the M2 helix [46,47]. Permeant ions probably access the transmembrane pore via the lateral fenestrations located just above the TMD [48,49].

By crosslinking 8-thiocyano-ATP (NCS-ATP) with single cysteine substitutions around the putative binding site, Jiang *et al*. [50] have now obtained evidence that NCS-ATP can bind in two opposite orientations (Figure 4). One has the adenine ring on the TMD proximal side of the four charge cluster (FCC) and the other has the ring on the TMD distal side. (A precedent for opposite ligand orientations was reported for an AChBP [51].) Interestingly, ATP-gated currents were potentiated by labeling NCS-ATP in the 'proximal' orientation but inhibited in the 'distal' orientation.

To elucidate a possible gating mechanism, Du *et al*. [4] carried out a normal mode analysis of the apo zP2X4R structure. A normal mode involving coupled motions of β1, β13, β14, and M2 was identified (see Figure Ic in Box 2). In particular, the pre-M2 loop expanded outward. The resulting widening of the fenestrations above the TMD and opening of the transmembrane pore bear signatures of channel activation. The authors then docked ATP near the FCC in two opposite orientations, with the adenine either proximal or distal to the TMD, and followed with parallel molecular dynamics simulations (Figure 4). In the simulations with the proximal orientation, the ATP molecule became wedged between β13 and β14 of one protomer

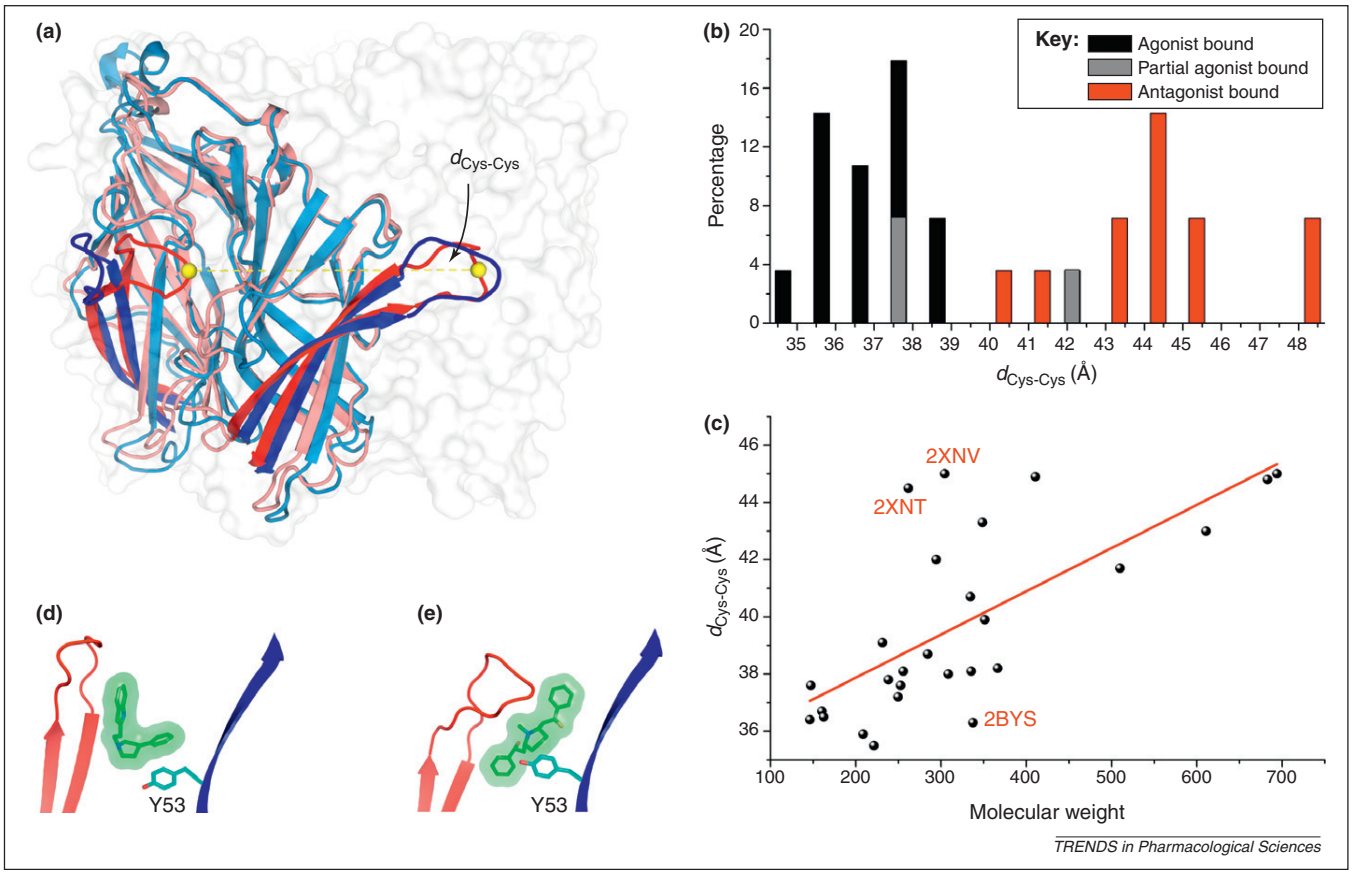

Figure 2. Ligand-induced conformational changes of nicotinic acetylcholine receptors (nAChRs). **(a)** Superposition of an agonist-bound acetylcholine-binding protein (AChBP) structure [Protein Data Bank (PDB) entry 1UW6] [15] (red) and an antagonist-bound AChBP structure (PDB entry 2BYP) [8] (blue). The inner β-sheets of the pentamer are used for superposition. Two of the five protomers are shown as cartoon; the remaining ones are shown as gray surface. C_α atoms of two Cys residues in neighboring C loops used for defining $d_{Cys-Cys}$ are shown as yellow spheres. (**b**) Histograms of nAChR agonists, partial agonists, and antagonists binned according to $d_{Cys-Cys}$. (**c**) Correlation between $d_{Cys-Cys}$ and ligand molecular weight. The PDB names of three outliers are given. (**d**) Compound 6 (shown as surface) bound to *Aplysia californica* AChBP (PDB entry 2XNV) [11]. The C loop is on the left and in red; β2 is on the right and in blue. (**e**) Lobeline bound to *Aplysia californica* AChBP (PDB entry 2BYS) [8].

and β1 of the neighboring protomer, acting as a fulcrum that turned modest closure of the FCC into significant outward expansion of the pre-M2 loop. The simulations thus hint at how ATP binding triggers channel activation. The gating mechanism suggested by the computational studies explains the potentiation effect of NCS-ATP labeled in the 'proximal' orientation as well as many other observations in functional studies (Box 2). Very recently, Hattori and Gouaux [52] determined a structure for zP2X4R in the ATP-bound form. This structure confirms key elements of the proposed gating mechanism, including an outward expansion of the pre-M2 loop. ATP is bound to a location similar to that in the simulations, but adopts a different conformation, with the adenine positioned to the

Box 2. Gating mechanisms of three families of LGICs

The understanding of ligand actions on the three families of LGICs requires an understanding of their gating mechanisms. To provide the basis for rationalizing the proposed correlation between ligand size and ligand action, the current knowledge on the propagation of motions from the LBDs to the TMDs and the gating motions of the TMDs is summarized below.

Many studies of Cys loop receptors have suggested that the β1–β2 loop, Cys loop, and M2–M3 linker, positioned at the LBD–TMD interface [1,16–18] (Figure Ia), are involved in propagating motions from the LBD to the TMD in triggering channel opening [59–70]. Using mutant cycle analysis, Sines and coworkers [64,69,70] identified a pathway, consisting of strongly coupled residues, for example, between V46 in the β1–β2 loop and P272 in the M2–M3 linker (muscle nAChR α protomer numbering), across the LBD–TMD interface. Based on rate equilibrium free energy relations, Auerbach and coworkers [59,63,68] further suggested that agonist binding generates a wave that propagates from the ligand-binding site to the β1–β2 loop and Cys loop, then to the M2–M3 linker, and finally down the M2 helix. The substituted cysteine accessibility method (SCAM) indicates that, upon channel activation, the lower end of β1 in α7 nAChR becomes less accessible but the lower end of β2 becomes more accessible [71]. Change in the propensity of substituted cysteines to form disulfide bonds between the β1–β2 loop and M2–M3 linker of a 5-HT_3 receptor suggests that these two elements move apart during channel activation [66].

Still unclear is the mechanism by which the motions at the ligand-binding site are propagated across the LBD–TMD interface to drive the outward tilt of the external end of the pore-lining M2 helix. An idea that has been repeatedly raised is that the resting state conformation is strained; agonist binding acts to relieve the strain and opens the pore as a result. Unwin [1] suggested that the strain is manifested by lack of 5-fold symmetry in the LBD of the muscle nAChR. Specifically, the two α protomers, whose C loops provide the ligand-binding sites, are rotated relative to the three non-α protomers. Lee *et al.* [69] considered the apo LBD as a brake that maintains a closed channel pore; ligand binding disengages the LBD from the TMD, allowing the pore to open. Similarly, Hilf and Dutzler [17] envisioned breaking an unidentified critical interaction in the LBD–TMD interface.

Figure Ib illustrates the mechanism of GluR2 AMPA receptor activation developed from targeted molecular dynamics simulations [33]. As previously suggested by Sobolevsky *et al.* [2], the outward motion of each 'distal' D2 tip drags the M3–D2 linker, which in turn pulls outward the external end of the pore-lining M3 helix, opening the pore and distorting the 4-fold symmetry. The whole TMD also moves upward, such that the D2 lobes stay anchored on top of the cell membrane. Moreover, the diagonal pairs of M3–D2 linkers rotate relative to each other in the lateral plane, so that the four linkers are positioned more in line with 4-fold symmetry. It is as though the abrupt transition between the 2-fold symmetry of the M3–D2 linkers and the 4-fold symmetry of the M3 helices in the resting state builds up a strain, which, upon agonist binding, drives the relative rotation between the proximal and distal pairs of M3–D2 linkers.

This activation model explains many observations in functional studies, including the pattern of agonist-induced accessibility changes from SCAM measurements of the M3 external portion [72]; the 2-fold symmetry of the outer pore in the activated state [73]; and the effect of M3–D2 linker charge mutations on channel desensitization [74]. One could now also see why the extent of ligand-induced LBD closure is correlated with the degree of channel activation [7,34]. As illustrated in Figure Ib, the closure of the D2 lobe is directly translated into the outward movement of the M3 external end and channel opening. Therefore, the greatest LBD closure, as induced by agonists, opens the channel to the greatest extent. Moderate closure of the LBD clamshells, as induced by partial agonists, opens the channel to a moderate extent. The open LBD conformation, as maintained by antagonists, keeps the channel closed.

By combining normal mode analysis and molecular dynamics simulations, Du *et al.* [4] developed a gating mechanism for P2X4R (described in the main text; Figure Ic). The atomistic model produced both a pattern of ATP-induced accessibility changes in M1 and M2 that is consistent with SCAM measurements [46,75] and the observed expansion of the lateral fenestrations [48]. It also explains why an interprotomer disulfide bond (presumably leading to interface closure) above the FCC potentiates the ATP-activated current [48], whereas a disulfide bond below the FCC has a reduced rate of formation in the presence of ATP [76].

A lipophilic compound ivermectin acts as a positive allosteric modulator of P2X4R. Ivermectin, extending ~20 Å in length, was suggested by mutational studies [77,78] to be inserted between the M1 and M2 helices. As shown in Figure Ic, the spacing between M1 and M2 increases upon channel opening, providing room for ivermectin. Therefore, by preferentially binding, ivermectin may stabilize the open state, as previously proposed [79]. A similar effect of ivermectin was established by the putative open structure of a GluCl channel with ivermectin wedged between the M1 and M3 helices of two neighboring protomers [29].

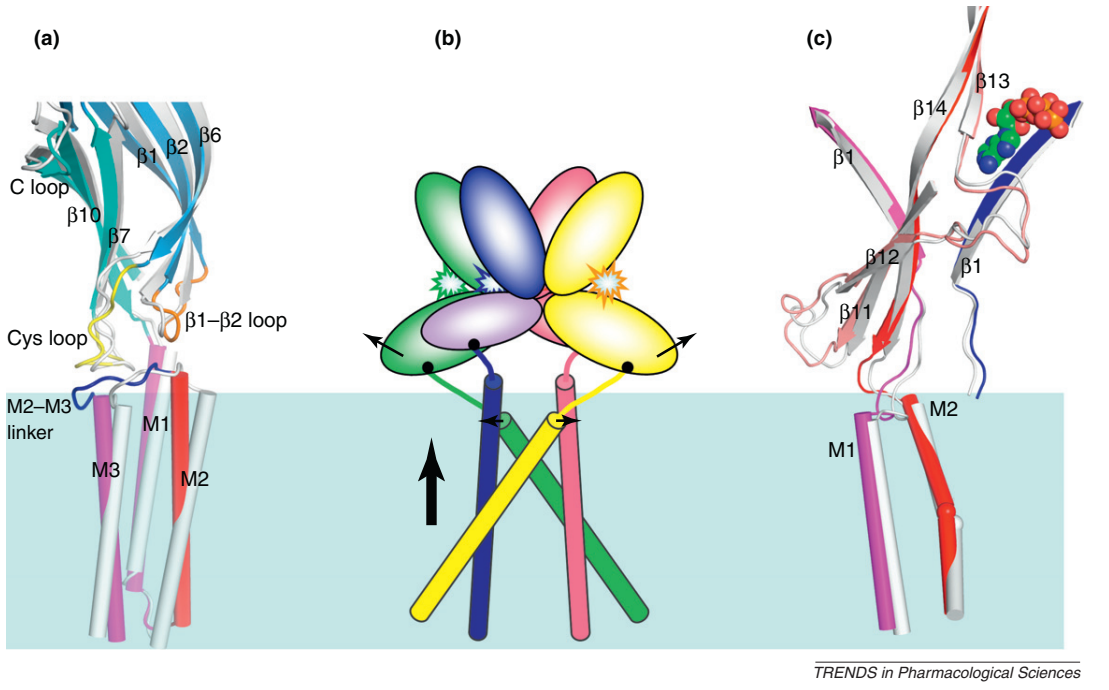

Figure I. Gating models for three families of ligand-gated ion channels. (**a**) Gating mechanism of Cys loop receptors as suggested by superimposing the structures of ELIC [Protein Data Bank (PDB) entry 2VL0] [16] (in gray) and GLIC (PDB entry 3EHZ) [17] (in color). The M1 helices of the pentamer are used for superposition. (**b**) Gating mechanism of ionotropic glutamate receptors suggested by targeted molecular dynamics simulations [33]. The four protomers have the same colors as in Figure 1c. Agonist-induced motions of the ligand-binding domain and transmembrane domain (TMD) are indicated by arrows. The D2 lobes move outward, pulling apart the outer portions of the M3 helices and listing up the TMD. (**c**) Gating mechanism of P2X receptors developed from normal mode analysis and molecular dynamics simulations [4]. The resting state is shown in gray; bound ATP is shown as spheres, and the activated state is shown in color. M2 becomes less bent in the activated state.

outside, not inside, of the triphosphate group. In the molecular dynamics simulations with the distal orientation, ATP appeared to stabilize the tightening of the surrounding trimeric interface and the closure of the pre-M2 loop, possibly representing a desensitized state.

Many P2XR antagonists have been identified [53–55], including a subtype nonselective, competitive antagonist called suramin. A mutational study [56] identified K138 in the human P2X1 receptor (corresponding to D141 in zP2X4R) as a possible suramin-interacting residue. In the zP2X4R structure, this residue is located on the distal side of the FCC (Figure 4b). This lends support to the suggestion that competitive antagonists may occupy the wider interprotomer ridge above the FCC (similar to ATP in the distal orientation), thereby maintaining the closure of the pre-M2 loop. Many other P2XR antagonists are described as noncompetitive, and their binding sites remain unknown [53–55].

Insight for designing pharmacological compounds

The three families of LGICs are involved in many human diseases and are known drug targets. Structural information and mechanistic understanding are undoubtedly

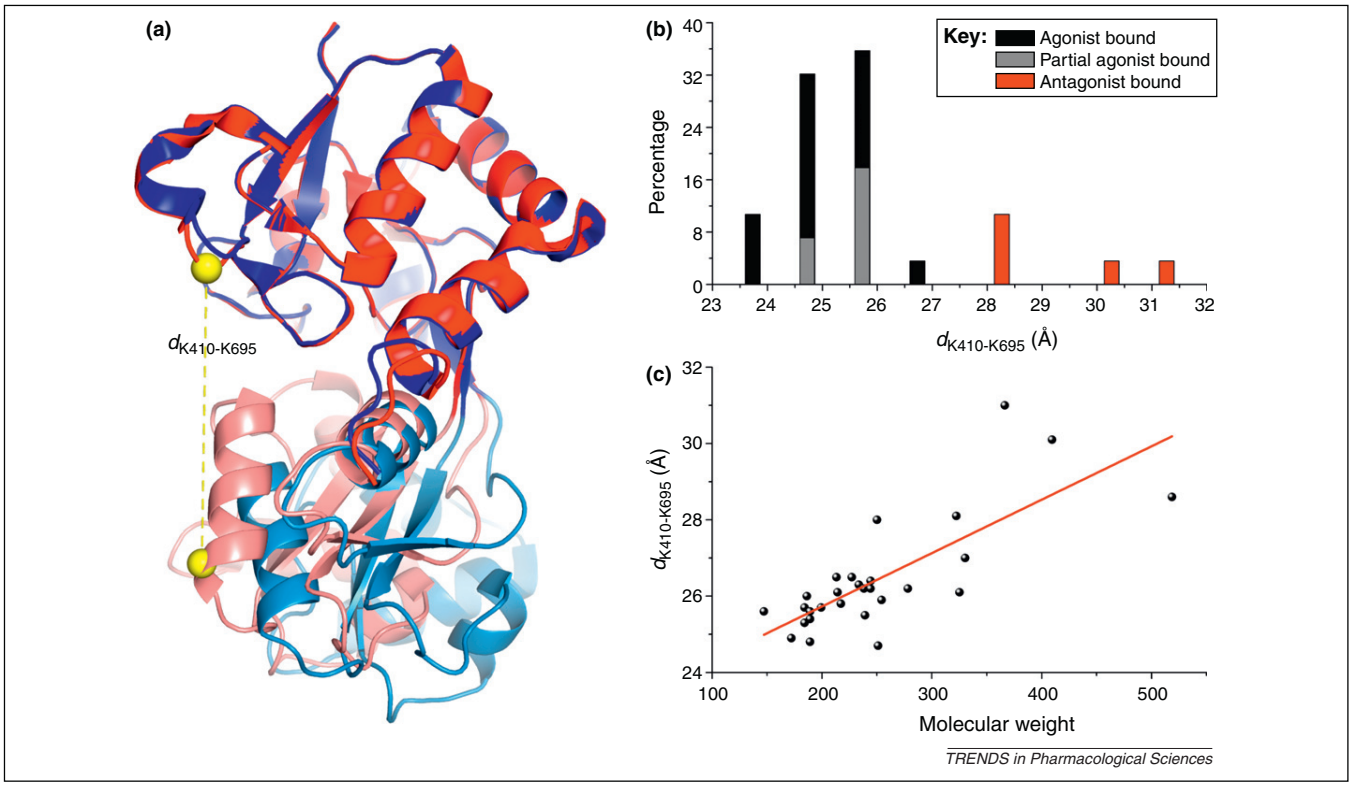

Figure 3. Ligand-induced conformational changes of glutamate receptors. **(a)** Superposition of an agonist-bound GluR2 ligand-binding domain (LBD) structure [Protein Data Bank (PDB) entry 1M5C] [96] (red) and an antagonist-bound structure (PDB entry 3R7X) [105] (blue). The D1 lobe of a protomer is used for superposition. C_α atoms of K410 in D1 (dark red) and K695 in D2 (light red) used for defining $d_{K410-K695}$ are shown as yellow spheres. (**b**) Histograms of α-amino-3-hydroxyl-5-methyl-4-isoxazole propionic acid (AMPA) receptor agonists, partial agonists, and antagonists binned according to $d_{K410-K695}$. (**c**) Correlation between $d_{K410-K695}$ and ligand molecular weight.

valuable for antagonist design. For both Cys loop receptors and iGluRs, it seems clear that competitive antagonism requires sufficient opening of the ligand-binding pocket, which in turn requires ligands with sufficient sizes. There are hints that the same may apply to P2XRs as well.

However, for ligands to become drugs, molecular weight (a measure of molecular size) is a premium. Compound 6, an α7 nAChR antagonist [11], points a way for eliciting maximal binding pocket opening with a minimal molecular weight. The wedge shape of the molecule is ideally suited to pry open the binding pocket. It will be interesting to see

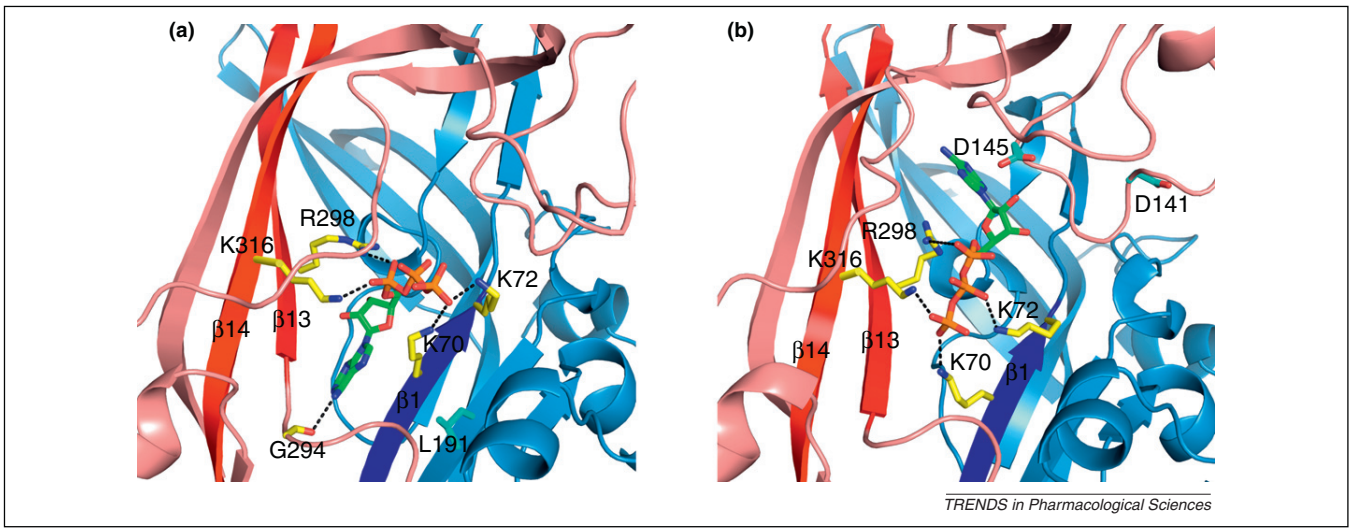

Figure 4. Two opposite ATP-binding orientations in P2X4 receptor, suggested by 8-thiocyano-ATP (NCS-ATP) labeling [50] and refined by molecular dynamics simulations [4]. (**a**) ATP bound in the 'proximal' orientation. Side chains of the four charge cluster, interacting with the triphosphate group, are shown. The backbone carbonyl of G294 forms a hydrogen bond with the adenine group. L191 corresponds to a position where NCS-ATP was labeled [50]. (**b**) ATP bound in the 'distal' orientation. D145 corresponds to a second position where NCS-ATP was labeled [50] The antagonist suramin perhaps binds in a similar mode. D141 corresponds to a position implicated in suramin binding [56].

whether the same design can be adapted for iGluR and P2XR antagonists.

With more and more structures available for the LGICs, *in silico* screening has become increasingly useful for identifying high-affinity ligands [11,57,58]. Experimental verification is essential. *In silico* screening by Akdemir *et al*. [11] successfully identified compound 6, but not the docking pose in the crystal structure (PDB 2XNV). In the docking simulation the ligand adopted an extended conformation, instead of the wedge-shaped folded conformation in the crystal structure.

Subtype selective antagonists are more useful as drug leads but are more challenging to design. Subtype specific residues lining the ligand binding pocket will have to be taken into consideration.

Concluding remarks

In this review, common lessons among the three families of LGICs have been emphasized. In all these LGICs, agonists induce closure of the binding pocket, whereas competitive antagonists seem to reverse the direction of motion; ligand size appears to be a key determinant of binding pocket motional direction. The gates of these LGICs all seem to be located at the outer portion of a helix, with outward tilting the likely gating motion (Box 2). For Cys loop receptors, the mechanism by which the binding pocket motion is transmitted to the gating motion has been controversial among many studies. Mechanistic models have recently been developed for the activation and desensitization of iGluRs [33] and P2XRs [4]. These probably will prompt additional studies and debate. The fact that the agonist-binding pocket can accommodate larger ligands (usually antagonists) means that some residues that could interact with ligands do not participate in interactions with agonists, and hence do not directly contribute to channel activation.

To move the field forward, integration of structure determination, functional study, and modeling and simulation will be important. Structures will continue to be the basis for modeling and simulation, and be indispensible for guiding functional studies. Modeling and simulation will be necessary to cover the chemical space of ligands and the subtype space of receptors. They can also be used to yield atomistic information on the activated state, which usually is too transient for structure determination. Structural comparison between the resting state and the activated state is valuable in many respects, in particular for understanding the action of allosteric modulators. Of course verification by functional studies remains essential.

Acknowledgments

This work was supported in part by National Institutes of Health grant GM58187.

References

1 Unwin, N. (2005) Refined structure of the nicotinic acetylcholine receptor at 4 Å resolution. *J. Mol. Biol.* 346, 967–989
2 Sobolevsky, A.I. *et al.* (2009) X-ray structure, symmetry and mechanism of an AMPA-subtype glutamate receptor. *Nature* 462, 745–756
3 Kawate, T. *et al.* (2009) Crystal structure of the ATP-gated P2X4 ion channel in the closed state. *Nature* 460, 592–598
4 Du, J. *et al.* (2012) Gating mechanism of a P2X4 receptor developed from normal mode analysis and molecular dynamics simulations. *Proc. Natl. Acad. Sci. U.S.A.* 109, 4140–4145
5 Brejc, K. *et al.* (2001) Crystal structure of an ACh-binding protein reveals the ligand-binding domain of nicotinic receptors. *Nature* 411, 269–276
6 Armstrong, N. *et al.* (1998) Structure of a glutamate-receptor ligand-binding core in complex with kainate. *Nature* 395, 913–917
7 Armstrong, N. and Gouaux, E. (2000) Mechanisms for activation and antagonism of an AMPA-sensitive glutamate receptor: crystal structures of the GluR2 ligand binding core. *Neuron* 28, 165–181
8 Hansen, S.B. *et al.* (2005) Structures of *Aplysia* AChBP complexes with nicotinic agonists and antagonists reveal distinctive binding interfaces and conformations. *EMBO J.* 24, 3635–3646
9 Brams, M. *et al.* (2011) A structural and mutagenic blueprint for molecular recognition of strychnine and *d*-tubocurarine by different Cys-loop receptors. *PLoS Biol.* 9, e1001034
10 Yi, M. *et al.* (2008) Spontaneous conformational change and toxin binding in α7 acetylcholine receptor: insight into channel activation and inhibition. *Proc. Natl. Acad. Sci. U.S.A.* 105, 8280–8285
11 Akdemir, A. *et al.* (2011) Acetylcholine binding protein (AChBP) as template for hierarchical *in silico* screening procedures to identify structurally novel ligands for the nicotinic receptors. *Bioorg. Med. Chem.* 19, 6107–6119
12 Brown, N. *et al.* (2002) Pharmacological characterization of a novel cell line expressing human $\alpha_4\beta_3\delta$ $GABA_A$ receptors. *Br. J. Pharmacol.* 136, 965–974
13 Bertrand, D. *et al.* (1992) Unconventional pharmacology of a neuronal nicotinic receptor mutated in the channel domain. *Proc. Natl. Acad. Sci. U.S.A.* 89, 1261–1265
14 Bertrand, S. *et al.* (1997) Paradoxical allosteric effects of competitive inhibitors on neuronal α7 nicotinic receptor mutants. *Neuroreport* 8, 3591–3596
15 Celie, P.H.N. *et al.* (2004) Nicotine and carbamylcholine binding to nicotinic acetylcholine receptors as studied in AChBP crystal structures. *Neuron* 41, 907–914
16 Hilf, R.J. and Dutzler, R. (2008) X-ray structure of a prokaryotic pentameric ligand-gated ion channel. *Nature* 452, 375–379
17 Hilf, R.J.C. and Dutzler, R. (2009) Structure of a potentially open state of a proton-activated pentameric ligand-gated ion channel. *Nature* 457, 115–118
18 Bocquet, N. *et al.* (2009) X-ray structure of a pentameric ligand-gated ion channel in an apparently open conformation. *Nature* 457, 111–114
19 Zimmermann, I. and Dutzler, R. (2011) Ligand activation of the prokaryotic pentameric ligand-gated ion channel ELIC. *PLoS Biol.* 9, e1001101
20 Zheng, W. and Auerbach, A. (2011) Decrypting the sequence of structural events during the gating transition of pentameric ligand-gated ion channels based on an interpolated elastic network model. *PLoS Comput. Biol.* 7, e1001046
21 Taly, A. *et al.* (2005) Normal mode analysis suggests a quaternary twist model for the nicotinic receptor gating mechanism. *Biophys. J.* 88, 3954–3965
22 Law, R.J. *et al.* (2005) A gating mechanism proposed from a simulation of a human α7 nicotinic acetylcholine receptor. *Proc. Natl. Acad. Sci. U.S.A.* 102, 6813–6818
23 Cheng, X. *et al.* (2006) Targeted molecular dynamics study of C-loop closure and channel gating in nicotinic receptors. *PLoS Comput. Biol.* 2, 1173–1184
24 Cheng, X. *et al.* (2007) Nanosecond-timescale conformational dynamics of the human α7 nicotinic acetylcholine receptor. *Biophys. J.* 93, 2622–2634
25 Zhu, F. and Hummer, G. (2009) Gating transition of pentameric ligand-gated ion channels. *Biophys. J.* 97, 2456–2463
26 Nury, H. *et al.* (2010) One-microsecond molecular dynamics simulation of channel gating in a nicotinic receptor homologue. *Proc. Natl. Acad. Sci. U.S.A.* 107, 6275–6280
27 Cymes, G.D. *et al.* (2005) Probing ion-channel pores one proton at a time. *Nature* 438, 975–980
28 Paas, Y. *et al.* (2005) Pore conformations and gating mechanism of a Cys-loop receptor. *Proc. Natl. Acad. Sci. U.S.A.* 102, 15877–15882
29 Hibbs, R.E. and Gouaux, E. (2011) Principles of activation and permeation in an anion-selective Cys-loop receptor. *Nature* 474, 54–60

30 Bartos, M. *et al.* (2009) Structural basis of activation of Cys-loop receptors: the extracellular-transmembrane interface as a coupling region. *Mol. Neurobiol.* 40, 236–252
31 Miller, P.S. and Smart, T.G. (2010) Binding, activation and modulation of Cys-loop receptors. *Trends Pharmacol. Sci.* 31, 161–174
32 Sun, Y. *et al.* (2002) Mechanism of glutamate receptor desensitization. *Nature* 417, 245–253
33 Dong, H. and Zhou, H-X. (2011) Atomistic mechanism for the activation and desensitization of an AMPA-subtype glutamate receptor. *Nat. Commun.* 2, 354
34 Jin, R. *et al.* (2003) Structural basis for partial agonist action at ionotropic glutamate receptors. *Nat. Neurosci.* 6, 803–810
35 Stern-Bach, Y. *et al.* (1998) A point mutation in the glutamate binding site blocks desensitization of AMPA receptors. *Neuron* 21, 907–918
36 Armstrong, N. *et al.* (2006) Measurement of conformational changes accompanying desensitization in an ionotropic glutamate receptor. *Cell* 127, 85–97
37 Gonzalez, J. *et al.* (2010) Role of dimer interface in activation and desensitization in AMPA receptors. *Proc. Natl. Acad. Sci. U.S.A.* 107, 9891–9896
38 Browne, L.E. *et al.* (2010) New structure enlivens interest in P2X receptors. *Trends Pharmacol. Sci.* 31, 229–237
39 Young, M.T. (2010) P2X receptors: dawn of the post-structure era. *Trends Biochem. Sci.* 35, 83–90
40 Ennion, S. *et al.* (2000) The role of positively charged amino acids in ATP recognition by human P2X1 receptors. *J. Biol. Chem.* 275, 29361–29367
41 Jiang, L-H. *et al.* (2000) Identification of amino acid residues contributing to the ATP-binding site of a purinergic P2X receptor. *J. Biol. Chem.* 275, 34190–34196
42 Wilkinson, W.J. *et al.* (2006) Role of ectodomain lysines in the subunits of the heteromeric P2X2/3 receptor. *Mol. Pharmacol.* 70, 1159–1163
43 Zemkova, H. *et al.* (2007) Role of aromatic and charged ectodomain residues in the P2X4 receptor functions. *J. Neurochem.* 102, 1139–1150
44 Fischer, W. *et al.* (2007) Conserved lysin and arginin residues in the extracellular loop of P2X3 receptors are involved in agonist binding. *Eur. J. Pharmacol.* 576, 7–17
45 Roberts, J.A. *et al.* (2008) Cysteine substitution mutagenesis and the effects of methanethiosulfonate reagents at P2X2 and P2X4 receptors support a core common mode of ATP action at P2X receptors. *J. Biol. Chem.* 283, 20126–20136
46 Li, M. *et al.* (2010) Pore-opening mechanism in trimeric P2X receptor channels. *Nat. Commun.* 1, 44
47 Kracun, S. *et al.* (2010) Gated access to the pore of a P2X receptor. *J. Biol. Chem.* 285, 10110–10121
48 Kawate, T. *et al.* (2011) Ion access pathway to the transmembrane pore in P2X receptor channels. *J. Gen. Physiol.* 137, 579–590
49 Samways, D.S.K. *et al.* (2011) Preferential use of unobstructed lateral portals as the access route to the pore of human ATP-gated ion channels (P2X receptors). *Proc. Natl. Acad. Sci. U.S.A.* 108, 13800–13805
50 Jiang, R. *et al.* (2011) Agonist trapped in ATP-binding sites of the P2X2 receptor. *Proc. Natl. Acad. Sci. U.S.A.* 108, 9066–9071
51 Tomizawa, M. *et al.* (2008) Atypical nicotinic agonist bound conformations conferring subtype selectivity. *Proc. Natl. Acad. Sci. U.S.A.* 105, 1728–1732
52 Hattori, M. and Gouaux, E. (2012) Molecular mechanism of ATP binding and ion channel activation in P2X receptors. *Nature* 485, 207–212
53 Evans, R.J. (2010) Structural interpretation of P2X receptor mutagenesis studies on drug action. *Br. J. Pharmacol.* 161, 961–971
54 Coddou, C. *et al.* (2011) Activation and regulation of purinergic P2X receptor channels. *Pharmacol. Rev.* 63, 641–683
55 Syed, N-i-H. and Kennedy, C. (2012) Pharmacology of P2X receptors. *WIREs Membr. Transp. Signal.* 1, 16–30
56 Sim, J.A. *et al.* (2008) Ectodomain lysines and suramin block of P2X1 receptors. *J. Biol. Chem.* 283, 29841–29846
57 Ulens, C. *et al.* (2009) Use of acetylcholine binding protein in the search for novel α7 nicotinic receptor ligands. In silico docking, pharmacological screening, and X-ray analysis. *J. Med. Chem.* 52, 2372–2383
58 Edink, E. *et al.* (2011) Fragment growing induces conformational changes in acetylcholine-binding protein: a structural and thermodynamic analysis. *J. Am. Chem. Soc.* 133, 5363–5371
59 Grosman, C. *et al.* (2000) Mapping the conformational wave of acetylcholine receptor channel gating. *Nature* 403, 773–776
60 Kash, T.L. *et al.* (2003) Coupling of agonist binding to channel gating in the $GABA_A$ receptor. *Nature* 421, 272–275
61 Miyazawa, A. *et al.* (2003) Structure and gating mechanism of the acetylcholine receptor pore. *Nature* 423, 949–955
62 Bouzat, C. *et al.* (2004) Coupling of agonist binding to channel gating in an ACh-binding protein linked to an ion channel. *Nature* 430, 896–900
63 Chakrapani, S. *et al.* (2004) Gating dynamics of the acetylcholine receptor extracellular domain. *J. Gen. Physiol.* 123, 341–356
64 Lee, W.Y. and Sine, S.M. (2005) Principal pathway coupling agonist binding to channel gating in nicotinic receptors. *Nature* 438, 243–247
65 Grutter, T. *et al.* (2005) Molecular tuning of fast gating in pentameric ligand-gated ion channels. *Proc. Natl. Acad. Sci. U.S.A.* 102, 18207–18212
66 Reeves, D.C. *et al.* (2005) A role for the β_1–β_2 loop in the gating of 5-HT_3 receptors. *J. Neurosci.* 25, 9358–9366
67 Xiu, X. *et al.* (2005) A unified view of the role of electrostatic interactions in modulating the gating of Cys loop receptors. *J. Biol. Chem.* 280, 41655–41666
68 Jha, A. *et al.* (2007) Acetylcholine receptor gating at extracellular transmembrane domain interface: the Cys-loop and M2-M3 linker. *J. Gen. Physiol.* 130, 547–558
69 Lee, W.Y. *et al.* (2008) Nicotinic receptor interloop proline anchors β1–β2 and Cys loops in coupling agonist binding to channel gating. *J. Gen. Physiol.* 132, 265–278
70 Lee, W.Y. *et al.* (2009) Binding to gating transduction in nicotinic receptors: Cys-loop energetically couples to pre-M1 and M2-M3 regions. *J. Neurosci.* 29, 3189–3199
71 McLaughlin, J.T. *et al.* (2007) Agonist-driven conformational changes in the inner β-sheet of α7 nicotinic receptors. *Mol. Pharmacol.* 71, 1312–1318
72 Sobolevsky, A.I. *et al.* (2003) Different gating mechanisms in glutamate receptor and K^+ channels. *J. Neurosci.* 23, 7559–7568
73 Sobolevsky, A.I. *et al.* (2004) The outer pore of the glutamate receptor channel has 2-fold rotational symmetry. *Neuron* 41, 367–378
74 Yelshansky, M.V. *et al.* (2004) Block of AMPA receptor desensitization by a point mutation outside the ligand-binding domain. *J. Neurosci.* 24, 4728–4736
75 Li, M. *et al.* (2008) Gating the pore of P2X receptor channels. *Nat. Neurosci.* 11, 883–887
76 Jiang, R. *et al.* (2010) A putative extracellular salt bridge at the subunit interface contributes to the ion channel function of the ATP-gated P2X2 receptor. *J. Biol. Chem.* 285, 15805–15815
77 Silberberg, S.D. *et al.* (2007) Ivermectin interaction with transmembrane helices reveals widespread rearrangements during opening of P2X receptor channels. *Neuron* 54, 263–274
78 Jelinkova, I. *et al.* (2008) Identification of $P2X_4$ receptor transmembrane residues contributing to channel gating and interaction with ivermectin. *Pflugers Arch.* 456, 939–950
79 Priel, A. and Silberberg, S.D. (2004) Mechanism of ivermectin facilitation of human P2X4 receptor channels. *J. Gen. Physiol.* 123, 281–293
80 Brams, M. *et al.* (2011) Crystal structures of a cysteine-modified mutant in loop D of acetylcholine-binding protein. *J. Biol. Chem.* 286, 4420–4428
81 Hibbs, R.E. *et al.* (2009) Structural determinants for interaction of partial agonists with acetylcholine binding protein and neuronal α7 nicotinic acetylcholine receptor. *EMBO J.* 28, 3040–3051
82 Celie, P.H.N. *et al.* (2005) Crystal structure of acetylcholine-binding protein from *Bulinus truncatus* reveals the conserved structural scaffold and sites of variation in nicotinic acetylcholine receptors. *J. Biol. Chem.* 280, 26457–26466
83 Ihara, M. *et al.* (2008) Crystal structures of *Lymnaea stagnalis* AChBP in complex with neonicotinoid insecticides imidacloprid and clothianidin. *Invert. Neurosci.* 8, 71–81
84 Talley, T.T. *et al.* (2008) Atomic interactions of neonicotinoid agonists with AChBP: molecular recognition of the distinctive electronegative pharmacophore. *Proc. Natl. Acad. Sci. U.S.A.* 105, 7606–7611

85 Bourne, Y. *et al.* (2010) Structural determinants in phycotoxins and AChBP conferring high affinity binding and nicotinic AChR antagonism. *Proc. Natl. Acad. Sci. U.S.A.* 107, 6076–6081
86 Nemecz, A. and Taylor, P.W. (2011) Creating an α7 nicotinic acetylcholine recognition domain from the acetylcholine binding protein: crystallographic and ligand selectivity analyses. *J. Biol. Chem.* 286, 42555–42565
87 Celie, P.H.N. *et al.* (2005) Crystal structure of nicotinic acetylcholine receptor homolog AChBP in complex with an α-conotoxin PnIA variant. *Nat. Struct. Mol. Biol.* 12, 582–588
88 Bourne, Y. *et al.* (2005) Crystal structure of a Cbtx–AChBP complex reveals essential interactions between snake α-neurotoxins and nicotinic receptors. *EMBO J.* 24, 1512–1522
89 Li, S.X. *et al.* (2011) Ligand-binding domain of an α_7-nicotinic receptor chimera and its complex with agonist. *Nat. Neurosci.* 14, 1253–1259
90 Weston, M.C. *et al.* (2006) Interdomain interactions in AMPA and kainate receptors regulate affinity for glutamate. *J. Neurosci.* 26, 7650–7658
91 Kasper, C. *et al.* (2002) GluR2 ligand-binding core complexes: importance of the isoxazolol moiety and 5-substituent for the binding mode of AMPA-type agonists. *FEBS Lett.* 531, 173–178
92 Frydenvang, K. *et al.* (2010) Biostructural and pharmacological studies of bicyclic analogues of the 3-isoxazolol glutamate receptor agonist ibotenic acid. *J. Med. Chem.* 53, 8354–8361
93 Armstrong, N. *et al.* (2003) Tuning activation of the AMPA-sensitive GluR2 ion channel by genetic adjustment of agonist-induced conformational changes. *Proc. Natl. Acad. Sci. U.S.A.* 100, 5736–5741
94 Jin, R. *et al.* (2002) Mechanism of activation and selectivity in a ligand-gated ion channel: structural and functional studies of GluR2 and quisqualate. *Biochemistry* 41, 15635–15643
95 Beich-Frandsen, M. *et al.* (2008) Structures of the ligand-binding core of iGluR2 in complex with the agonists (R)- and (S)-2-amino-3-(4-hydroxy-1,2,5-thiadiazol-3-yl)propionic acid explain their unusual equipotency. *J. Med. Chem.* 51, 1459–1463
96 Hogner, A. *et al.* (2002) Structural basis for AMPA receptor activation and ligand selectivity: crystal structures of five agonist complexes with the GluR2 ligand-binding core. *J. Mol. Biol.* 322, 93–109
97 Lunn, M-L. *et al.* (2003) Three-dimensional structure of the ligand-binding core of GluR2 in complex with the agonist (S)-ATPA: implications for receptor subunit selectivity. *J. Med. Chem.* 46, 872–875
98 Poon, K. *et al.* (2011) Mechanisms of modal activation of GluA3 receptors. *Mol. Pharmacol.* 80, 49–59
99 Nielsen, B.B. *et al.* (2005) Exploring the GluR2 ligand-binding core in complex with the bicyclical AMPA analogue (S)-4-AHCP. *FEBS J.* 272, 1639–1648
100 Frandsen, A. *et al.* (2005) Tyr702 is an important determinant of agonist binding and domain closure of the ligand-binding core of GluR2. *Mol. Pharmacol.* 67, 703–713
101 Holm, M.M. *et al.* (2005) Structural determinants of agonist-specific kinetics at the ionotropic glutamate receptor 2. *Proc. Natl. Acad. Sci. U.S.A.* 102, 12053–12058
102 Jin, R. and Gouaux, E. (2003) Probing the function, conformational plasticity, and dimer–dimer contacts of the GluR2 ligand-binding core: studies of 5-substituted willardiines and GluR2 S1S2 in the crystal. *Biochemistry* 42, 5201–5213
103 Hogner, A. *et al.* (2002) Competitive antagonism of AMPA receptors by ligands of different classes: crystal structure of ATPO bound to the GluR2 ligand-binding core, in comparison with DNQX. *J. Med. Chem.* 46, 214–221
104 Vogensen, S.B. *et al.* (2007) A tetrazolyl-substituted subtype-selective AMPA receptor agonist. *J. Med. Chem.* 50, 2408–2414
105 Koller, M. *et al.* (2011) Quinazolinedione sulfonamides: a novel class of competitive AMPA receptor antagonists with oral activity. *Bioorg. Med. Chem. Lett.* 21, 3358–3361
106 Kasper, C. *et al.* (2006) The structure of a mixed GluR2 ligand-binding core dimer in complex with (S)-glutamate and the antagonist (S)-NS1209. *J. Mol. Biol.* 357, 1184–1201